Surface-dependent sulfidation and orientation of MoS_2 slabs on alumina-supported model HDS catalysts

Cédric Bara,[a, b] Anne-Félicie Lamic-Humblot,[a] Emiliano Fonda,[c] Anne-Sophie Gay,[b] Anne-Lise Taleb,[b] Elodie Devers,[b] Mathieu Digne,[b] Gerhard D. Pirngruber[b] and Xavier Carrier*[a]

[a] Sorbonne Universités, UPMC Univ Paris 06, UMR CNRS 7197, Laboratoire de Réactivité de Surface, F-75005, Paris, France

[b] IFP Energies nouvelles, BP3, Rond Point échangeur de Solaize, F-69360 Solaize, France

[c] Synchrotron SOLEIL, F-91192, Gif-sur-Yvette, France

Corresponding Author

* Email address: xavier.carrier@upmc.fr; Tel: +33 1 44 27 36 25; Fax: +33 1 44 27 60 33.

Abstract

The constant improvement of hydrotreating (HDT) catalysts, driven by industrial and environmental needs, requires a better understanding of the interactions between the oxide support (mostly alumina) and the MoS_2 active phase. Hence, this work addresses the support-dependent genesis of MoS_2 on four planar, single crystal α-Al_2O_3 surfaces with different crystal orientations (C (0001), R ($1\bar{1}02$), M ($10\bar{1}0$) and A ($11\bar{2}0$)). In contrast to classical surface science techniques, which often rely on UHV-type deposition methods, the Mo is introduced by impregnation from an aqueous solution, in order to mimic the standard incipient wetness impregnation. Comparison between different preparation routes, impregnation vs. equilibrium adsorption (selective adsorption), is also considered. AFM, XAS, TEM and XPS show that the α-Al_2O_3 orientation has a clear impact on the strength of metal-support interactions at the oxide state with consequences on the sulfidation, size, stacking and orientation of MoS_2 slabs. Aggregation of molybdenum oxide particles is observed on the C (0001) plane suggesting weak metal-support interactions leading to high sulfidation degree with large slabs. Conversely, the presence of well-dispersed individual oxide particles on the R ($1\bar{1}02$) plane implies stronger metal-support interactions leading to a low sulfidation degree and shorter MoS_2 slabs. Both A ($11\bar{2}0$) and M ($10\bar{1}0$) facets, of similar crystallographic structure, display an intermediate behaviors in terms of sulfidation rate and MoS_2 size in line with intermediary metal-support interactions. Polarization-dependent Grazing-Incidence-EXAFS experiments as well as HR HAADF-STEM analysis allow us to demonstrate a surface-dependent orientation of MoS_2 slabs. A predominant basal bonding is suggested on the C (0001) plane in agreement with the existence of weak metal-support interactions. Conversely, a random orientation (edge and basal-bonding) is observed for the other planes. Generalization of these conclusions to industrial catalysts is proposed based on the comparison of the surface structure of the various model α-Al_2O_3 orientations used in this work and the predominantly exposed γ-Al_2O_3 surfaces ((110), (100) and (111)).

Introduction

Heterogeneous catalysts based on Transition Metal Sulfides (TMS) have long been used to eliminate heteroatoms (S, O, N) and metals from crude oil or petroleum fraction for environmental reasons (to decrease polluting gas emission during oil combustion) but also for industrial concerns in order to protect catalysts used downstream in the refinery [1]. Among all impurities, sulfur represents a major problem since it leads to sulfur dioxide emission, responsible of acid rain and catalytic converter poisoning [2]. Therefore, legislation on the maximum tolerated sulfur content in fuels is more and more stringent which implies a constant improvement of hydrotreating catalysts. More recently, TMS-based catalysts have also attracted a great interest for biomass processing as hydrogenation/decarboxylation catalysts for renewable lipids and hydrodeoxygenation of pyrolysis oils from 2nd generation lignocellulosic biomass [3].

TMS-based heterogeneous catalysts are classically described as made of molybdenum or tungsten sulfide slabs ($Mo(W)S_2$) promoted at the edge by Co or Ni atoms,dispersed over a porous polycrystalline oxide support of high surface area, mostly γ-alumina [1,4–6]. One important and still largely debated question concentrates on the role of the oxide support on the sulfide active phase in terms of size, morphology, orientation or sulfidation degree. Even subtle differences, such as alumina polymorphism, have been shown to be a decisive factor. As a matter of fact, it has been demonstrated that promoted CoMoS catalysts supported on δ-Al_2O_3 show a higher intrinsic activity (per Mo atoms) than the same system supported on γ-Al_2O_3 [7]. These differences were explained in terms of better dispersion for the MoS_2 active phase and weaker metal-support interactions on δ-Al_2O_3. However, a rational understanding of these differences is excluded in industrial catalysts due to the use of high surface area, polycrystalline oxide particles that expose a variety of crystallographic planes with numerous defects and a multiplicity of surface hydroxyl groups. Yet, a molecular-scale understanding of the support influence is obviously a pre-requisite for a scientific design of industrial hydrotreating catalysts.

Surface-science type studies can help resolving this issue by using planar surfaces with well-controlled surface structure [8]. Specific reactivity of various surface orientations can thus be studied and compared to polycrystalline industrial materials. Specifically, Sakashita and Yoneda [9,10] studied non-promoted sulfided Mo catalysts on oriented Al_2O_3 thin films

prepared by electron beam evaporation of α-Al_2O_3 onto $MgAl_2O_4$ wafers. These authors claimed that MoS_2 slabs are oriented parallel to the support on the most predominant γ-Al_2O_3 (110) surface and show the highest sulfidation degree with respect to the other (100) and (111) orientations. However, the use of thin films epitaxially grown on an oriented substrate as models for γ-Al_2O_3 has been questioned [8]. More recently, we showed that α-alumina single crystals can be used as a suitable model for γ-Al_2O_3 since there are many analogies between the surface structure of γ-Al_2O_3, the metastable polycrystalline industrial support, and α-Al_2O_3, the thermodynamically stable alumina polymorph from which single crystal wafers can be grown [8,11].

We have recently followed this surface-science approach using well defined α-alumina single crystal wafers of different orientations (i.e A $(11\bar{2}0)$, C (0001), M $(10\bar{1}0)$ and R $(1\bar{1}02)$ planes) combined with an aqueous-phase deposition method of Mo denoted equilibrium adsorption (or selective adsorption). The deposition from aqueous phase is closer to industrial procedures of catalysts preparation than more classical UHV surface science deposition methods [11]. It was shown that the surface speciation of alumina hydroxyls controls the Mo adsorption at the oxide/water interface and in turn the strength of metal-support interactions leading to various sulfidation degrees depending on the surface orientation. Structural analogies between α and γ alumina allow the following extrapolation to polycrystalline supports: we can expect a heterogeneous Mo distribution over industrial γ-Al_2O_3 supported catalysts, with a strong metal-support interaction and low sulfidation degree on the predominant (110) surface, and lower metal-support interactions, but higher sulfidation degrees on the (111) and (100) planes.

To step forward in understanding industrial catalysts, the present contribution broadens the previous approach by using an alternative aqueous-phase deposition method, i.e. a simple *impregnation* (without filtration and washing steps), which mimics the classical *incipient wetness impregnation* (also known as dry impregnation) used with shaped oxide supports. This method has two advantages with respect to equilibrium/selective adsorption: first weakly reactive surfaces (such as the C (0001) plane in the present case) [11] can be used since weakly interacting Mo species will not be washed out with a rinsing step and second, the amount of deposited Mo can be easily controlled so that various orientations with identical Mo surface density can be prepared. Hence, model catalysts have been prepared on various α-alumina single crystal wafers (A $(11\bar{2}0)$, C (0001), M $(10\bar{1}0)$ and R $(1\bar{1}02)$ planes) and

sulfided at different temperatures to study the role of each α-alumina surface on the nature of the active phase: sulfidation degree, MoS_2 nanoparticle size and metal-support interaction with XPS, AFM and TEM. The orientation of the active phase has also been investigated by surface EXAFS spectroscopy and high resolution scanning transmission electron microscopy in high angle annular dark field mode (HR HAADF-STEM). The role of the synthesis route toward Mo adsorption and sulfidation is finally discussed with respect to the surface hydroxyl speciation.

Materials and Methods

Preparation of model catalysts ($MoOx/\alpha$-Al_2O_3)

1 cm^2 single crystal α-alumina wafers were purchased from Mateck for the A $(11\bar{2}0)$, C (0001) and R $(1\bar{1}02)$ planes and from SurfaceNet for the M $(10\bar{1}0)$ orientation. The wafers were first chemically cleaned with successive washing steps in water, HNO_3 and NH_3 following a procedure already reported in ref [11]. A final calcination step was performed in air in a muffle furnace overnight at 700 °C. Mo impregnation was carried out through deposition of a 100 µL droplet of an aqueous solution of ammonium heptamolybdate tetrahydrate, $(NH_4)_6Mo_7O_{24}.4H_2O$ (Merck, > 99% purity) at the natural pH (5.2) of the solution. Two different Mo surface loadings were considered: 3.5 $at.nm^{-2}$ ([Mo] = $5.8.10^{-6}$ $mol.L^{-1}$) and 0.9 $at.nm^{-2}$ ([Mo] = $1{,}5.10^{-6}$ $mol.L^{-1}$) in order to be close to the surface saturation of the A $(11\bar{2}0)$ and M $(10\bar{1}0)$ planes (about 4 $at.nm^{-2}$) or the R $(1\bar{1}02)$ plane (1 $at.nm^{-2}$) as shown in ref [11]. Most of the results presented in the paper focus on the highest surface concentration (3.5 $at.nm^{-2}$). After Mo deposition, the model catalysts were dried 1 h at room temperature under primary vacuum to remove the solvent. It was also noticed that this step favored a homogeneous spreading of the 100 µL droplet over the wafer. After drying, samples were calcined 2 h at 450 °C in air in a muffle furnace.

Sulfidation of model catalysts (MoS_2/α-Al_2O_3)

Conventional gas phase sulfidation was performed in a glass reactor under a flow of 2 $L.h^{-1}$ of 15 mol% H_2S/H_2 at atmospheric pressure and constant temperature (100, 200, 300, 400 or 450 °C) for 2 h. The reactor was then cooled down to 80 or 150 °C (depending on sulfidation temperature) for 1 h under argon (2 $L.h^{-1}$) to remove any excess of sulfur. Catalysts were then kept under argon at room-temperature before analysis.

Characterization

XPS: XPS spectra were recorded with an Omicron (ESCA+) instrument using a monochromatic Al X-ray source (hν = 1486.6 eV) with an accelerating voltage of 14 kV and a current intensity of 20 mA (overall energy resolution was about 0.8 eV). Spectra were collected at a takeoff angle of 90° under a pressure lower than10^{-9} mbar. More information can be found in ref [11]. XPS was used to quantify the sulfidation degree through the methodology developed by Gandubert et *al*. [12] by integrating the contributions of MoS_2, MoO_xS_y and MoO_3. The sulfidation degree (% MoS_2) was calculated as the ratio of the contribution of MoS_2 over the total contribution of Mo (MoS_2 + MoO_xS_y + MoO_3). Sulfided samples were rapidly transferred (less than 1 min.) from the sulfidation reactor to the XPS analysis chamber and it was checked that this fast transfer prevents any reoxidation of MoS_2.

TEM: Conventional TEM images were collected with a JEOL 2010 microscope operating at 200 kV for determining the average size (length of a fringe) and stacking (number of fringes) of MoS_2 particles using *ImageJ 1.45* software [13]. TEM samples were obtained by scratching the surface with a razor blade in order to concentrate the clusters of active phase into an ethanol drop before spreading this drop on a carbon-coated copper grid.
High-resolution high angle annular dark field scanning transmission electron microscopy (HR HAADF-STEM) analyses were performed using a JEOL 2100 F FEG TEM/STEM instrument operating at 200 kV, equipped with a Cs aberration probe corrector. For HAADF acquisition, the camera length was 10 cm corresponding to inner and outer diameters of annular detector of about 60 and 160 mrad. Model catalysts (MoS_2/α-Al_2O_3wafers) were scratched with a diamond tip scriber. The as obtained alumina fragments were suspended in ethanol and sonicated. A drop of the suspension was deposited on a Cu grid covered with a holey carbon membrane.

AFM: Topographic AFM images on MoS_2/α-Al_2O_3 samples were obtained on a Nanoscope VIII Multimode AFM from Bruker Nano Inc. (Nano Surfaces Division, Santa Barbara, CA) equipped with a 150 x 150 x 5 μm^3 scanner (J-scanner). AFM analyses were performed using the peak force tapping mode (PFT), recently developed [14] with silicon tip on Si_3N_4 cantilevers. It was checked that no significant evolution of morphology occured during AFM imaging. The root mean square surface roughness (R_{rms}) is expressed by the square root of the sum of the squares of the individual heights and depths from the mean line.

X-ray absorption: Surface EXAFS in Grazing-Incidence geometry (Grazing-Incidence X-ray Absorption Spectroscopy or GI-XAS) was conducted on the SAMBA beamline at the SOLEIL synchrotron facility (Saint-Aubin, France) [15]. Spectra were collected in the fluorescence mode with a Canberra 36 pixels solid-state Ge detector at the Mo K edge (20 keV). The orientation of the wafers was varied with respect to the polarization of the synchrotron beam. These orientations will be denoted parallel and perpendicular throughout the text when the electric-field vector of the synchrotron beam is respectively parallel and perpendicular to the surface of the wafer.

For sulfide samples, planar catalysts were transferred from the sulfidation reactor to the EXAFS sample holder in a glove box and then fixed with carbon tape on a goniometer head in a sealed plastic box filled with argon in order to prevent any oxidation. Reference compounds were collected in transmission mode by diluting the samples in cellulose. XAS data analysis was carried out with the Demeter package [16].

It has to be noted that coordination numbers reported in this paper are *effective* coordination numbers as defined by Equ. 1 [17] that depend on the polarization of the synchrotron beam. For example, the effective coordination numbers ($N_{effective}$) will be three times higher than the actual number of neighbors (N_{real}) when the chemical bond (directed along $\vec{r}$) is parallel to the electric field vector $\vec{\epsilon}$ ($\cos\theta = 1$).

Equ. 1 $$N_{effective}(\theta) = \sum_{i=1}^{Nreal} 3[\vec{\varepsilon}.\vec{r}]^2 = 3\sum_{i=1}^{Nreal} \cos(\theta)^2$$

Results and Discussion

1. Molybdenum oxide dispersion: AFM

AFM images were recorded after aqueous-phase impregnation of Mo (high loading 3.5 at.nm^{-2}) on A ($11\bar{2}0$), C (0001), M ($10\bar{1}0$) and R ($1\bar{1}02$) planes and subsequent calcination at 450°C in order to investigate the Mo dispersion at the oxide state. Surface roughness analysis, before Mo deposition, shows a relatively smooth surface for all orientations (i.e. R_{rms} of 0.10-0.15 ± 0.01 nm). However, succeeding impregnation and calcination lead to three different behaviors depending on the surface orientation (Figure 1).

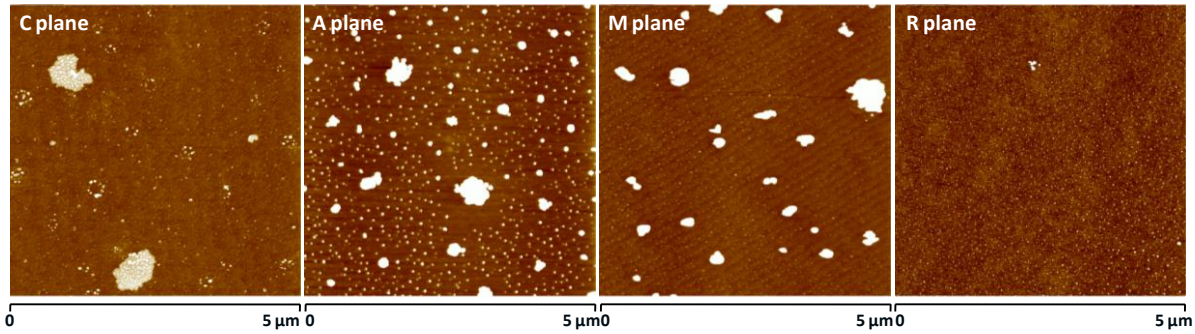

Figure 1: Representative AFM images (5 x 5 µm^2, Peak Force Tapping mode, z-scale 4 nm) of planar Mo/α-Al_2O_3 model catalysts with a Mo surface loading of 3.5 at.nm^{-2} after impregnation and calcination at 450 °C for 2 h for various alumina orientations: C (0001), A ($11\bar{2}0$), M ($10\bar{1}0$) and R ($1\bar{1}02$) planes.

On the C (0001) plane, a large part of the Mo oxide particles are aggregated forming large clusters with a width of 600 to 900 nm. These clusters are composed of a collection of individual particles about 7 to 22 nm wide and 1 to 4 nm high. The remaining alumina surface is mostly free of Mo even if few individual nanoparticles are still discernable. Only a slight increase of the surface roughness is observed up to 0.40 ± 0.01 nm since large parts of the wafer are uncovered leading to a heterogeneous distribution of Mo on the C (0001) surface. On A ($11\bar{2}0$) and M ($10\bar{1}0$) planes, a drastic increase of the surface roughness is observed up to 4.0 ± 0.01 nm due to the presence of two sets of nanoparticles: aggregates (average height of 20-70 nm and width of 100-500 nm) and individual particles (average height of 1-9 nm and width of 5-30 nm). The M ($10\bar{1}0$) plane slightly differs from the A ($11\bar{2}0$) plane by the presence of steps (0.2 to 0.3 nm high). This faceting behavior has already been observed by others after high temperature treatment [18–20] but Mo oxide nanoparticles are not specifically located along these steps. On the R ($1\bar{1}02$) plane, no aggregation is observed and small Mo oxide nanoparticles (average height of 1-4 nm and width of 2-11 nm) are homogeneously distributed on the surface. Hence, the surface roughness increases only slightly (0.30 ± 0.01 nm) with respect to the bare surface (0.15± 0.01 nm).

The aggregation of molybdenum oxide nanoparticles observed with AFM can be taken as a good indication of the strength of metal-support interactions at the oxide state [21–23]. The homogeneous distribution of small nanoparticles on the R ($1\bar{1}02$) plane reveals strong metal-support interactions responsible of nanoparticle stabilization. Conversely, low metal-support interactions on the C (0001) plane leads to a large aggregation of particles [24]. A ($11\bar{2}0$) and

M ($10\bar{1}0$) orientations exhibit an intermediate behavior with stabilization of one group of oxide particles and sintering of the other group. These results are in full agreement with our previous work on A ($11\bar{2}0$), M ($10\bar{1}0$) and R ($1\bar{1}02$) planes after selective adsorption of Mo but it completes the conclusions to the C (0001) plane which was not adsorbing Mo through equilibrium adsorption [11].

2. Molecular structure of the oxide phase: GI-XAS

The structure of Mo oxide nanoparticles obtained after calcination (high loading 3.5 at.nm^{-2}) was investigated using grazing-incidence X-ray absorption specroscopy (GI-XAS) by varying the orientation of the wafers with respect to the polarization of the synchrotron beam (parallel vs perpendicular). First, Mo coordination was determined by comparing the XANES region of the model catalysts with Mo reference compounds where Mo is 6-fold coordinated (ammonium heptamolybdate, noted AHM and molybdenum trioxide, noted MoO_3) or 4-fold coordinated (sodium molybdate, Na_2MoO_4). Octahedral or tetrahedral coordinations show distinct features in the pre-edge region (1s to 4d transition at 20 000-20 010 eV, Figure 2) with enhanced intensity for four-fold coordination [25].

Figure 2 clearly shows that for all model catalysts, the pre-edge XANES feature is similar to the reference compounds where Mo is in octaedral coordination (i.e AHM and MoO_3) which rules out a tetrahedral symmetry for Mo. A closer look at the edge region also shows that model catalysts show three successive maxima at 20 023, 20 037 and 20 053 eV (Figure 2) whose positions and relative intensities are in good agreement with AHM features. Thus, it can be concluded that the speciation of molybdenum in the oxide state is relatively similar on A ($11\bar{2}0$), C (0001), M ($10\bar{1}0$) and R ($1\bar{1}02$) planes which can be explained by the presence of polymolybdate-like species with Mo located in edge-shared octahedral [25,26].

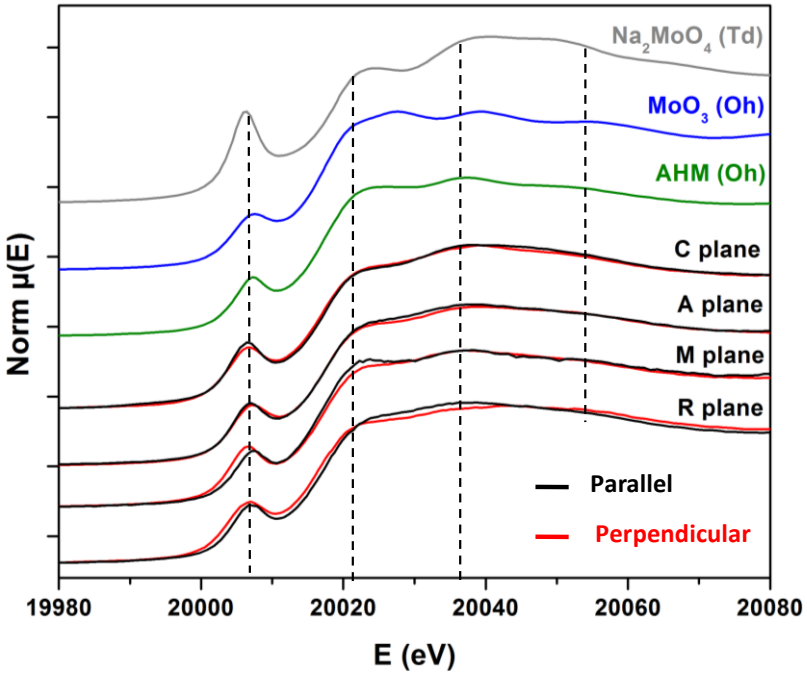

Figure 2: Mo K-edge XANES spectra of reference compounds and model Mo catalysts in parallel (black curve) and perpendicular (red curve) orientations with respect to the electric-field vector of the synchrotron beam. Model catalysts are supported on the C (0001), A ($11\bar{2}0$), M ($10\bar{1}0$) and R ($1\bar{1}02$) planes of α-Al_2O_3. Samples were prepared by Mo impregnation (high loading 3.5 at.nm^{-2}) and calcination at 450°C for 2h. (Norm μ(E): normalized absorption).

More specific information on a potential surface-dependent orientation of supported polymolybdate species can be obtained by comparing the spectra when the electric field vector of the synchrotron beam is set parallel or perpendicular to the surface of the single crystal wafer. In the case of an oriented adsorption of polymolybdate on the surface, the XANES region should exhibit dissimilarities between both polarizations [27–29] since Mo atoms are non equivalent in polyoxomolybdate species and each of them contributes directly to the relative intensity of the different maxima [25].

For the C (0001), A ($11\bar{2}0$) and M ($10\bar{1}0$) planes, no or very minor changes are discernible in the global XANES shape when the polarization is changed (Figure 2) suggesting that molybdates species are not specifically oriented on these three facets. One weak maximum is observed at 20 023 eV for the M ($10\bar{1}0$) plane in parallel polarization along with a slight shift of the pre-edge maximum. However, these small differences should not be overinterpreted since this spectrum is contaminated with numerous diffraction peaks from the alumina substrate throughout the energy range that modify the overall shape of the spectrum.

Conversely, on the R $(1\bar{1}02)$ plane, modest but discernable changes can be observed throughout the XANES region for the parallel and perpendicular polarizations: width of the pre-edge region and relative intensity between 20 020 and 20 040 eV. These differences suggest that molybdates species are specifically oriented on this surface in agreement with a previous work from Tougerti et *al*. [27] for Ni adsorption on the same surface.

This polarization dependence is further demonstrated by examination of both the EXAFS part (Figure 3a) and the Fourier-Transform of the EXAFS region for the R $(1\bar{1}02)$ surface for both polarizations (Figure 3b). In Figure 3b (Fourier Transforms), the relative intensity of the first peak at 1.2 Å corresponding to the Mo-O shell is more intense for the perpendicular polarization. Furthermore, the second shell (Mo-Mo) is only visible in this perpendicular polarization. For the sake of comparison, the FT of AHM has been reported and the second coordination shell (Mo-Mo) displays also two maxima at slightly lower Mo-Mo distances (i.e 2.7 and 3.2 Å) with a shoulder on the first peak. This pattern has been explained in the literature by the presence of three different types of Mo atoms in AHM with four different Mo-Mo distances from 3.19 to 3.43 Å [30,31].

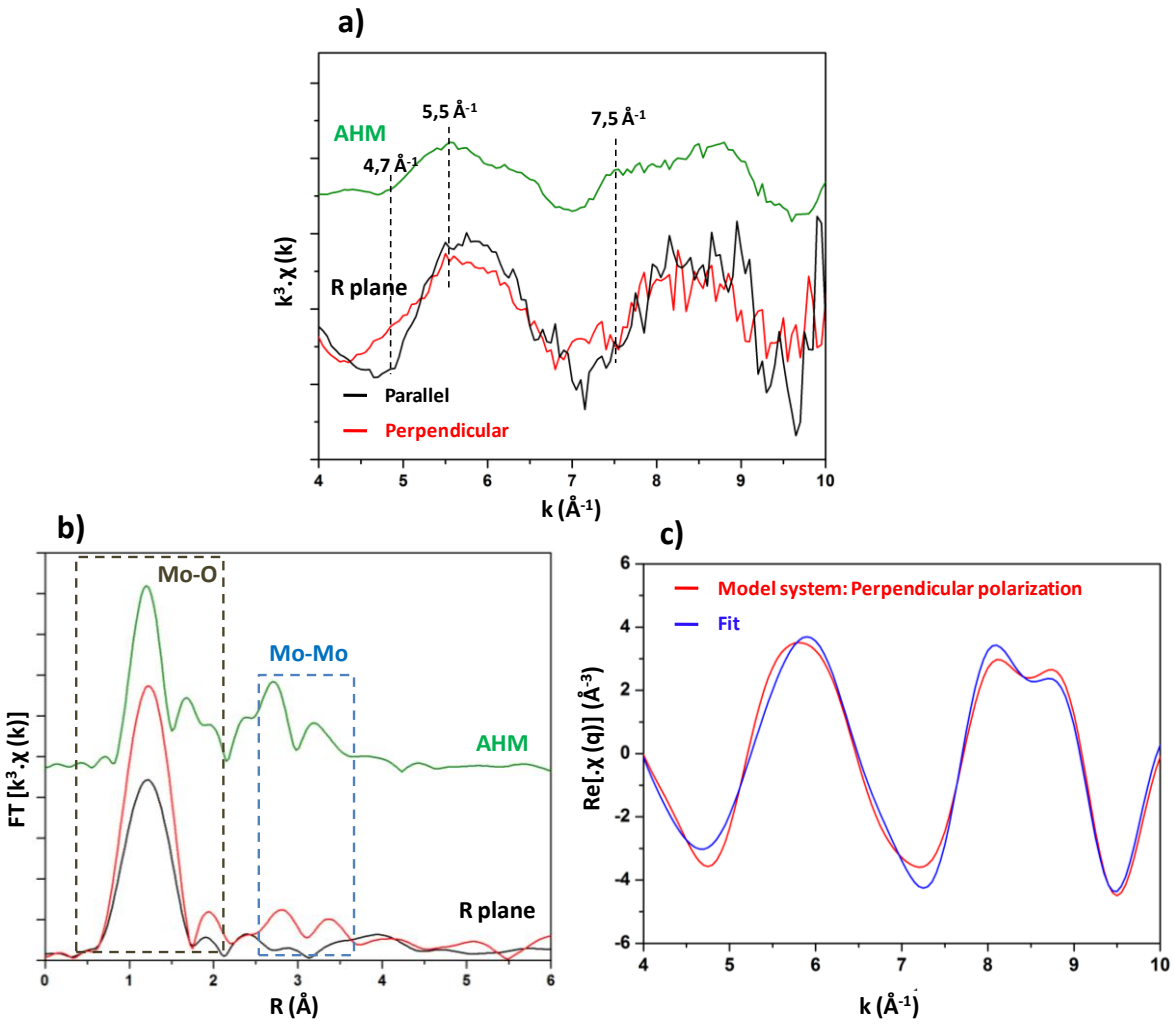

Figure 3: a) k^3-weighted Mo K-edge EXAFS spectra for Mo/α-Al_2O_3on the R ($1\bar{1}02$) plane calcined at 450°C for 2 h in parallel (black curve) and perpendicular (red curve) polarizations as well as for Ammonium Heptamolybdate (AHM, green curve), b) Corresponding Fourier transforms (Δk = 4-10 $Å^{-1}$) uncorrected for phase shift and c) the real part of the Fourier-filtered FT (ΔR = 1.0-3.6 Å) of the model catalyst in perpendicular polarization (red curve) and best fit (blue curve).

Table 1: EXAFS fitting results of the Fourier filtered (Δk = 4-10 $Å^{-1}$, ΔR = 1.0-3.6 Å) EXAFS signal for the parallel and perpendicular polarizations of the model catalyst Mo/α-Al_2O_3 on the R ($1\bar{1}02$) plane. N are effective coordination numbers. Only one σ^2 are fitted for the two Mo-Mo shells in perpendicular polarization and a single ΔE_0 value for all shells. Standard errors in EXAFS are N ± 20%, R ± 0.04 Å, $\Delta\sigma^2$ ± 20% and ΔE_0 ± 10%.

Polarization	**Shell**	**N**	**σ^2 ($Å^2$)**	**R (Å)**	**ΔE_0 (eV)**	**R-factor**
Parallel	Mo-O	2.0	0.003	1.77	-2.2	2.10^{-2}

Perpendicular	Mo-O	3.6	0.003	1.77	-1.1	
	Mo-Mo1	0.6	0.002	3.21	-1.1	2.10^{-2}
	Mo-Mo2	0.6	0.002	3.41	-1.1	

Qantitative analysis of the EXAFS results was performed by fitting the spectra obtained on the R $(1\bar{1}02)$ surface in the range of ΔR = 1.0-3.6 Å (Table 1). The Mo-O shell can been fitted with one O contribution at 1.77 Å with coordination numbers of 2.0 (parallel) and 3.6 (perpendicular) depending on the polarization. In fact, the variety of Mo-O distances in polymolybdates is responsible of constructive and destructive interferences in the EXAFS signal leading to a challenging determination of the number of oxygens neighbors [32–34]. Nevertheless, the clear difference shown for the two polarizations strongly suggests that the polymolybdate-like species are more extended in the perpendicular direction.

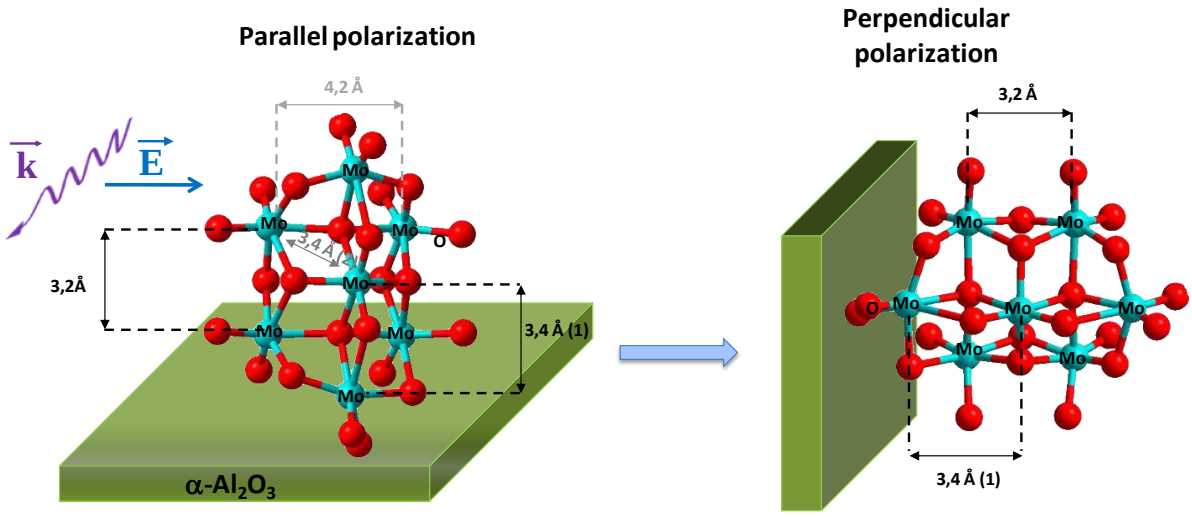

Scheme 1: "Edge-on" orientation of an heptamolybdate-like species on the R $(1\bar{1}02)$ plane of α-Al_2O_3. $\vec{k}$ is the wave vector and $\vec{E}$ is the electric field vector of the synchrotron beam. Parallel and perpendicular polarizations refer to the orientation of $\vec{E}$ with respect to the surface of the wafer.

The second shell can be fitted with two Mo contributions at 3.21 and 3.41 Å with similar coordination numbers of 0.6 (Figure 3c, Table 1). These results are in good agreement with those obtained for Mo catalysts supported on alumina powders [31]. The presence of Mo-Mo contributions only on the FT in perpendicular polarization is also in favor of a specific orientation of the polymolybdates. If one takes into account the structure of heptamolybdate, Mo-Mo bonds at 3.2 and 3.4 Å are indeed present (scheme 1). Of course, pure heptamolybdate species do no exist anymore as such on the surface after calcination but

XANES analysis showed that polymolybdate-like species are predominant and heptamolybdate can be taken as a simplified model of these surface polymolybdates. If one considers an orientation "edge-on" of the polymolybdate on the surface (i.e. adsorption via the smaller edge of the polyoxo compound), Mo-Mo bonds at 3.2 and 3.4 Å will be parallel to the electric field vector in perpendicular polarization (right on scheme 1) which will explain a strong enhancement of their contribution in the EXAFS signal [28]. Conversely, extinction of these Mo-Mo contributions will occur in parallel polarization since Mo-Mo bonds at 3.2 and 3.4 Å will be perpendicular to the electric field vector (left on scheme 1).

The EXAFS analysis points to a structuring effect of the R $(1\bar{1}02)$ plane on Mo surface species at the oxide state. On this surface, enhanced contributions of the Mo-O and Mo-Mo shells in perpendicular polarization suggest that molybdenum polyoxo clusters are more extended in the perpendicular direction as schematically represented on Scheme 1. This effect can be related to the conclusions drawn from AFM measurements (vide supra) that demonstrated the strongest metal-support interactions on the R $(1\bar{1}02)$ plane.

In the following sections, the influence of the oxide support on the genesis and orientation of the active phase (i.e molybdenum sulfide) will be discussed.

3. Genesis of the molybdenum sulfide active phase

Sulfidation is a crucial step in the catalyst synthesis route since it transforms the catalytically inactive molybdenum oxide phase into the active sulfide phase (i.e MoS_2). Metal-support interactions play a key role at this step which requires sulfidation of Mo-O-Al linkages (if anay) to substitute oxygen atoms by sulfur atoms [10,35–37]. Hence, different metal-support interactions should eventually lead to different sulfidation degrees.

Calcined model catalysts supported on A $(11\bar{2}0)$, C (0001), M $(10\bar{1}0)$ and R $(1\bar{1}02)$ planes with a Mo loading of 3.5 at.nm^{-2} were sulfided in gas phase (15 % H_2S/H_2) at several temperatures from 100 to 450 °C. Quantification of the sulfidation degree was performed by XPS spectroscopy based on the decomposition of Mo3d, S2s and S2p peaks taking into account the occurrence of three different Mo species: molybdenum oxide (MoO_3), molybdenum oxysulfide (MoO_xS_y) and molybdenum sulfide (MoS_2) [38,39]. An example of the decomposition of XPS spectra is shown in Figure 4 for a model catalyst sulfided at 450 °C and supported on the M $(10\bar{1}0)$ plane. The S2p peak can be decomposed in two contributions

at 161.8 and 163.3 ± 0.1 eV assigned to S^{2-} species involved in the MoS_2 phase and S_2^{2-} species related to oxysulfide compounds respectively [39]. The 220-230 eV region is composed of five contributions. Three of them at 228.9, 230.3 and 232.8 ± 0.1 eV are assigned to Mo3d for MoS_2, MoO_xS_y and MoO_3 respectively in good agreement with literature data [38,39]. The two other contributions at lower binding energy (i.e 226.0 and 227.5 ± 0.1 eV) are ascribed to S2s contributions (S^{2-} and S_2^{2-} respectively) in agreement with the S2p photopeak.

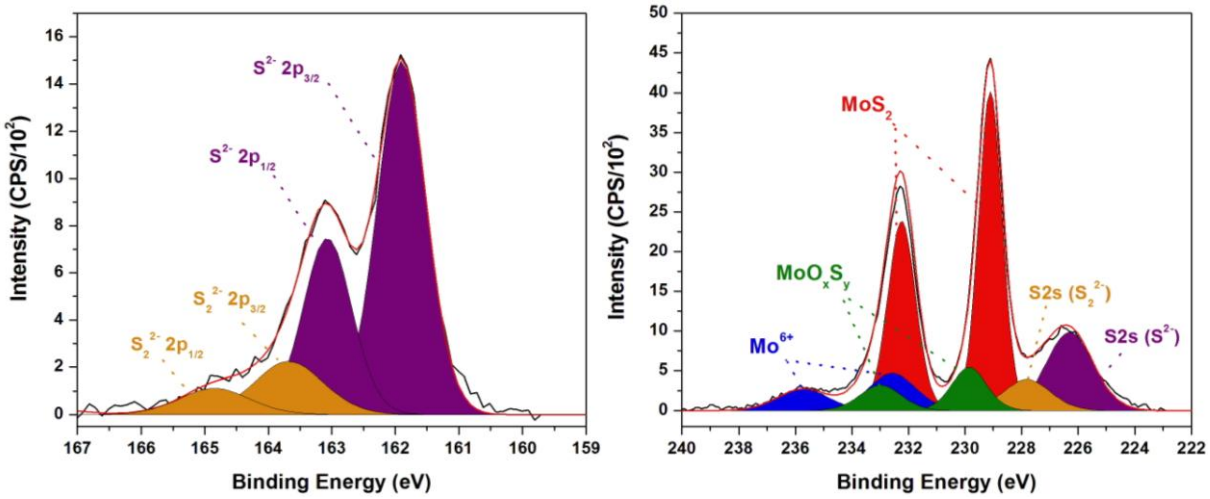

Figure 4: Decomposition of S2p, Mo3d and S2s XPS peaks for a model Mo/α-Al_2O_3 catalyst supported on the M $(10\bar{1}0)$ plane (3.5 atMo/nm²) and sulfided at 450 °C for 2 h.

Following this general procedure, the sulfidation degree (i.e. relative contribution of MoS_2 to the total contribution of Mo) has been determined for each model catalyst at different sulfidation temperatures (Figure 5). For all catalysts, sulfidation starts at low temperature (100 °C) and reaches about 90 % at 450 °C in good agreement with conventional supported catalysts [12]. One main difference among all model catalysts comes from a much higher sulfidation degree (53 %) at 100 °C on the C (0001) surface as compared to the other orientations (15-30 %) and to conventional catalysts [12]. Similarly, a maximum sulfidation degree of 90 % is reached as soon as 300°C on the C (0001) plane whereas the same ratio is only achieved at 450 °C for the other facets.

These results can be connected to different strengths of metal-support interactions as explained above. Namely, weak metal-support interactions at the oxide state on the C (0001) plane can explain extensive sulfidation at low temperature. These results are in line with the AFM results and also with the negligible reactivity of the C (0001) plane toward Mo or Ni

adsorption previously reported [11,27]. Al_{6c}-μ_2-OH surface hydroxyls wich are the only adsorption sites present on the C (0001) plane [11] form weak bonds with the polyoxo clusters which explains a full sulfidation at much lower temperature than the other alumina orientations.

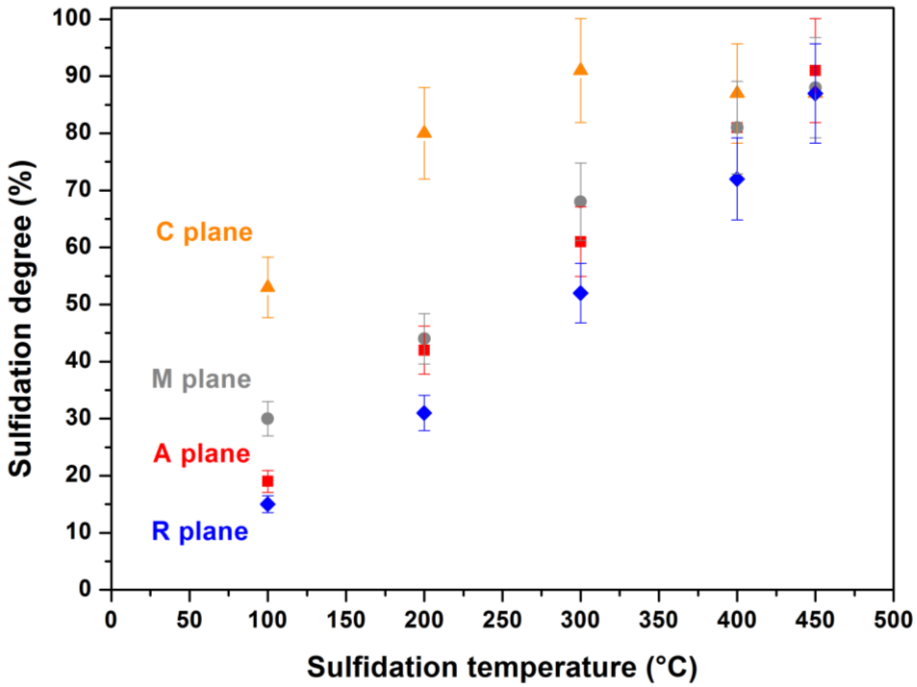

Figure 5: Sulfidation degree for model Mo/α-Al_2O_3 catalysts supported on C (0001), A ($11\bar{2}0$), M ($10\bar{1}0$) and R ($1\bar{1}02$) planes as a function of sulfidation temperature with a Mo surface loading of 3.5 at.nm^{-2}.

A ($11\bar{2}0$) and M ($10\bar{1}0$) planes display similar sulfidation degree (except at 100 °C where a difference is observed). Moreover, as a general trend, these two surfaces show a slightly higher sulfidation degree as compared to the R ($1\bar{1}02$) plane while these differences level off at 450°C. This conclusion is also in agreement with AFM results that showed stronger metal-support interactions at the oxide state for the R ($1\bar{1}02$) plane. This is also in line with the structuring effect of this latter surface for Mo oxide species observed with EXAFS. Moreover, these results derived from catalysts prepared by impregnation are also in full agreement with our previous results obtained for catalysts prepared by selective adsorption [11].

Stronger metal-support interactions on the R ($1\bar{1}02$) plane were explained by the speciation of surface hydroxyls, Al_{4c}-μ_1-OH, that will favor stronger bonds with the oxide phase leading to smaller oxide particles well dispersed and anchored to the surface and hardly sulfidable.

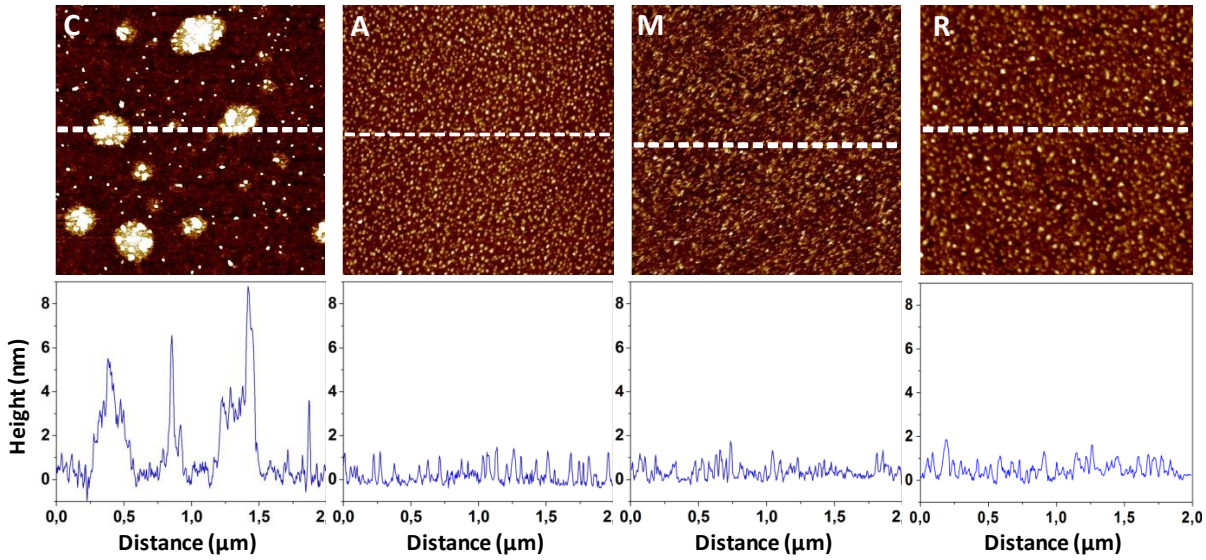

Figure 6: Representative AFM images (2.0 × 2.0 µm^2, peak force tapping mode in air, z-scale 8.0 nm) obtained on model Mo/α-Al_2O_3 catalysts supported on C (0001), R ($1\bar{1}02$), A ($11\bar{2}0$) and M ($10\bar{1}0$) planes and sulfided at 450 °C (Mo surface loading is 3.5 at.nm^{-2}). Cross sections were taken at the position indicated by the white dashed lines on the images.

AFM images (Figure 6) obtained on sulfided samples at 450°C show a homogeneous dispersion of MoS_2 nanoparticles for A ($11\bar{2}0$), M ($10\bar{1}0$) and R ($1\bar{1}02$) planes whereas large aggregates are observed on the C (0001) plane in agreement with the large clusters previously detected on this surface at the oxide state (Figure 1). Examination of cross section profiles confirms a similar and homogeneous particle density on A ($11\bar{2}0$), M ($10\bar{1}0$) and R ($1\bar{1}02$) orientations with an average particle height of 1-1.5 nm while a highly heterogeneous distribution is observed on the C (0001) plane with larger particles in height (2-8 nm).

It has also to be noted that comparison of Figure 1 (oxide state) and Figure 6 (sulfide state) shows a spreading of Mo particles during sulfidation for A ($11\bar{2}0$) and M ($10\bar{1}0$) planes. Aggregates observed at the oxide state, are no longer present after sulfidation. This behavior may be related to intermediate metal-support interactions as suggested by the different results reported above. Following recent in-situ TEM results [40], we may infer that small particles are probably sulfided first and then grow by adding Mo from larger particles (layer-by-layer growth).

TEM analysis was performed to confirm the influence of the support orientation on the size (length of the fringes) and stacking of MoS_2 slabs. Model catalysts were sulfided at 300 °C only, since XPS results (Figure 5) showed that differences among the various orientations in

term of sulfidation degree are smoothed at higher temperatures. Size distributions determined from TEM images (Figure 7) are presented on Figure 8. The trends are following those observed for the sulfidation degree: the highest average size (5,1 ± 0.1 nm) is obtained for the C (0001) plane with an important proportion of MoS_2 slabs (34 %) having a length above 5 nm, the lowest size (3,7 ± 0.1 nm) for the R ($1\bar{1}02$) plane and intermediate but similar sizes (4.1-4.2 ± 0.1 nm) are obtained for the A ($11\bar{2}0$) and M ($10\bar{1}0$) surfaces. Hence, both AFM and TEM reveal larger MoS_2 particles on the C (0001) plane.

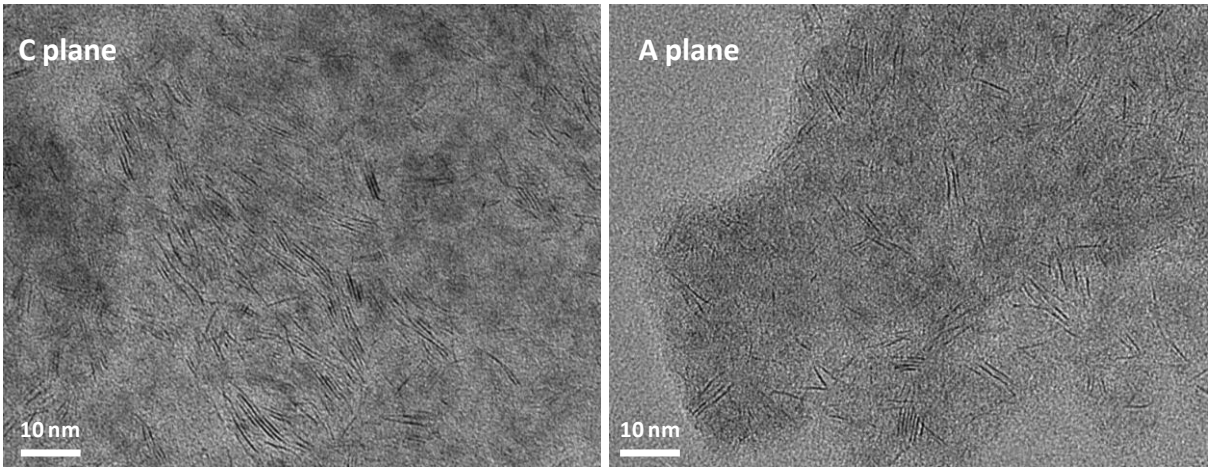

Figure 7: Typical TEM images of model Mo/α-Al_2O_3 catalysts supported on A ($11\bar{2}0$) and C (0001) planes sulfided at 300°C in H_2S/H_2 (Mo surface loading is 3.5 at.nm^{-2}).

The stacking distribution (Figure 8) does not change drastically between the four crystallographic orientations. However, it can be noticed that the C (0001) plane displays a slightly higher stacking degree which is also visible in Figure 7. This result is in agreement with Sakashita [10] who showed that aggregates at the oxide state lead to highly stacked slabs after sulfidation. AFM data indicate also a larger height for MoS_2 clusters on the C (0001) plane, which means higher stacking if one considers a basal bonding of MoS_2 nanoparticles.

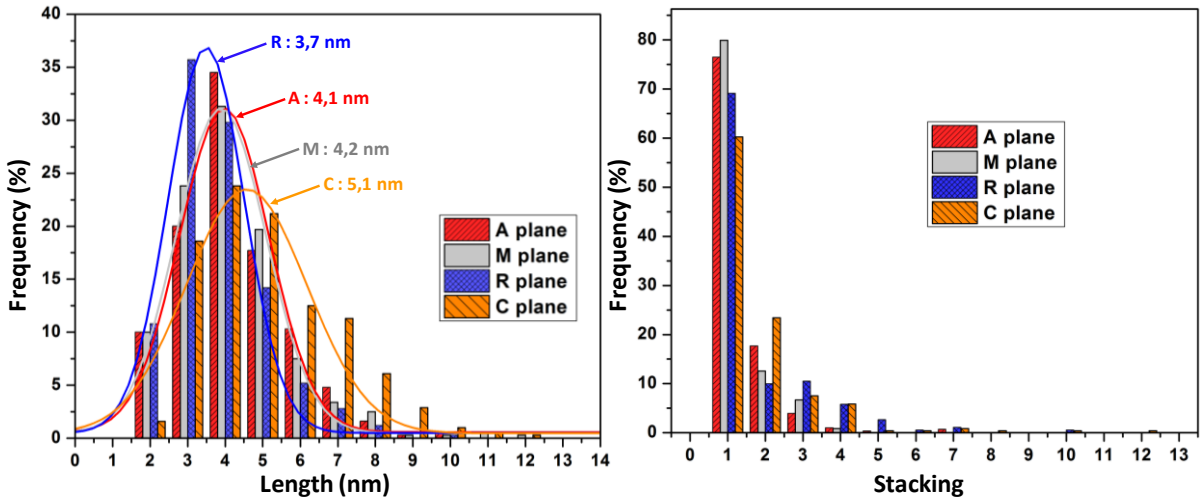

Figure 8: MoS_2 size and stacking distribution for model Mo/α-Al_2O_3catalysts supported on C (0001), R ($1\bar{1}02$), A ($11\bar{2}0$) and M ($10\bar{1}0$) planes sulfided at 300°C in H_2S/H_2 (Mo surface loading is 3.5 at.nm^{-2}).

AFM and GI-XAS for the oxide state as well as XPS, AFM and TEM for the sulfide state have shown that the structure, dispersion, size and sulfidation degree of model Mo/α-Al_2O_3 catalysts are highly depending on the alumina support orientation which is governing the strength of metal-support interactions.Weak metal-support interactions on the C (0001) plane lead to the formation of Mo oxide aggregates which are easily sulfidable into larger and stacked MoS_2 slabs. Intermediate metal-support interactions (A ($11\bar{2}0$) and M ($10\bar{1}0$) planes) induce a better dispersion of the oxide phase which will spread after sulfidation into smaller MoS_2 nanoparticles. Finally, strong metal-support interactions on the R ($1\bar{1}02$) plane generate a well-dispersed and oriented Mo oxide phase which is harder to sulfide and provide the smallest MoS_2 slabs. These differences can be related to the hydroxyl speciation on each surface which plays a key role on metal-support interactions as shown before [11]. The C (0001) plane exposes only Al_{6c}-μ_2-OH, A ($11\bar{2}0$) and M ($10\bar{1}0$) planes display three types of hydroxyl groups (i.e. Al_{6c}-$\mu_{1,2,3}$-OH) while the R ($1\bar{1}02$) surface exhibit Al_{4c}-μ_1-OH surface sites only.

In order to obtain information on the orientation of MoS_2 slabs, model catalysts have been further investigated at the sulfide state by GI-XAS and HAADF-STEM.

4. Support effect on the orientation of MoS_2 slabs

As for TEM analysis, model catalysts were sulfided at 300 °C under $H_2S(15\%)/H_2$ before GI-EXAFS experiments and analyzed using two polarizations (i.e parallel and perpendicular) as discussed previously for the oxide phase.

Mo K-edge XANES spectra of sulfided model catalysts are compared to bulk MoS_2 in Figure 9. The spectrum of the latter reference compound (blue curve, Figure 9) shows a shoulder at 20 014 eV and a single broad band at 20 032 eV in agreement with literature data [41]. The global shape of the XANES spectra of Mo/α-Al_2O_3 model catalysts exhibit similar features confirming sulfidation as shown above with XPS (Figure 5) [32,42,43]. Partial erosion of the shoulder at 20 014 eV also confirms that a full sulfidation has not been reached for all model catalysts as expected from the sulfidation temperature (i.e 300 °C) [44].

Very small polarization effects can be distinguished for the A $(11\bar{2}0)$, M $(10\bar{1}0)$ and R $(1\bar{1}02)$ orientations (Figure 9) which implies that there is no or little preferential orientation of the MoS_2 phase on these surfaces. Conversely, a more pronounced polarization effect appears for the C (0001) plane with an erosion of the shoulder at 20 014 eV and a more intense broad band at 20 032 eV for the perpendicular polarization. It is interesting to note at this point that there is no direct and simple relation for the orientation of Mo clusters between the oxide and sulfide state. In fact, GI-XAS experiments at the oxide state showed a preferential orientation of polyoxomolybdate on the R $(1\bar{1}02)$ plane and random orientation on the C (0001) plane while the situation is exactly reversed after sulfidation.

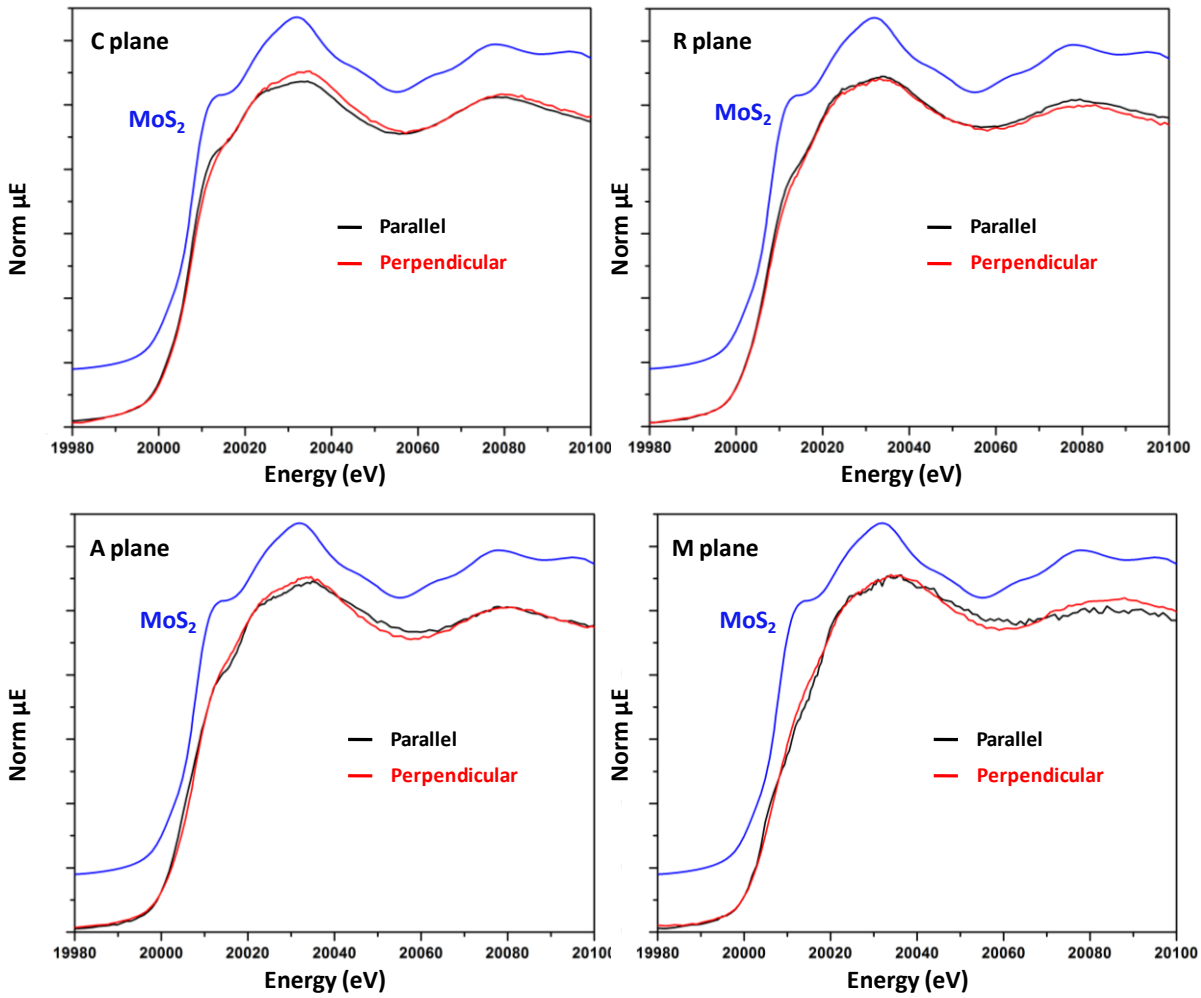

Figure 9: Mo-K edge XANES spectra of bulk MoS_2 (blue curve) and sulfided model Mo/α-Al_2O_3 catalysts in parallel (black curve) and perpendicular (red curve) polarizations supported on the C (0001), A ($11\bar{2}0$), M ($10\bar{1}0$) and R ($1\bar{1}02$) planes. Samples were prepared by Mo impregnation with a Mo surface loading of 3.5 at.nm^{-2}, calcination at 450°C for 2h and sulfidation at 300 °C under H_2S/H_2 (Norm µ(E): normalized absorption).

The EXAFS spectrum as well as the corresponding Fourier Transform (FT) for the model catalyst supported on the R ($1\bar{1}02$) plane are shown as an example in Figure 10 and compared to those for MoS_2. The EXAFS signal (Figure 10a) of the model catalyst is qualitatively in agreement with that of MoS_2 but obviously less structured (lack of shoulders at 5.0, 6.7 and 7.3 Å^{-1}) in agreement with a partial sulfidation at 300°C and weaker crystallinity. The corresponding FT for both samples (Figure 10b) shows a first shell at about 2 Å due to the first S neighbors (Mo-S single scattering path, 6 sulfur neighbors for bulk MoS_2) and a second shell at about 2.8 Å assigned to second Mo neighbors (Mo-Mo single scattering path, 6 Mo neighbors for bulk MoS_2). The FT of the model catalyst shows a weak second shell in

agreement with reported data for supported MoS_2 due to the small size and low crystallinity of these particles [41,45]. More quantitative information was obtained by fitting the experimental spectra for the model catalysts (see supporting information). All model catalysts can be fitted with a first shell at 2.36 Å with a coordination number between 2.4 and 5.3 and a second shell at 3.16 Å with a coordination number between 0.8 and 2.1. These data are in line with results reported for conventional catalysts supported on γ-alumina [46–50].

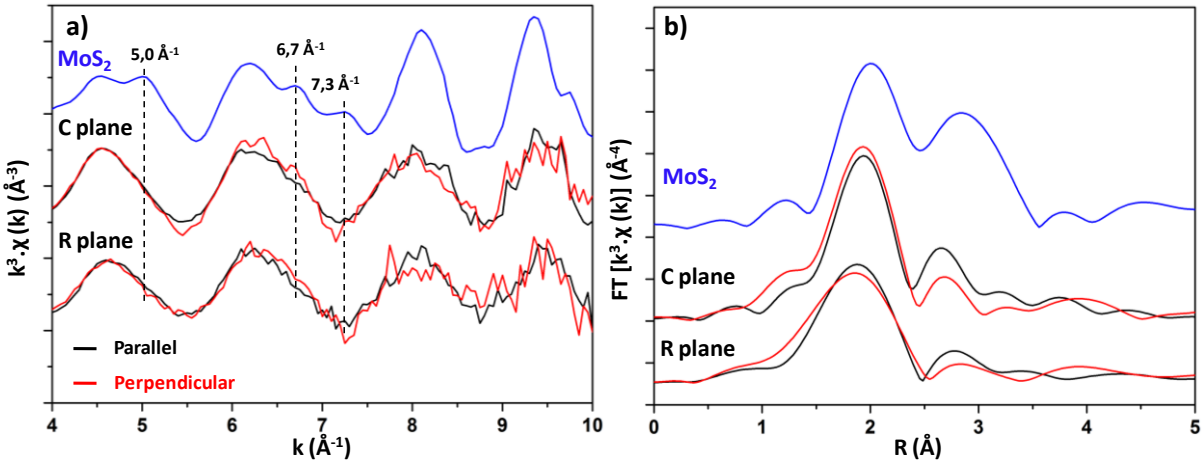

Figure 10: a) k^3-weighted Mo K-edge EXAFS spectra of bulk MoS_2 (blue curve) and sulfided model Mo/α-Al_2O_3 catalysts (Mo surface loading is 3.5 at.nm^{-2}) supported on the C (0001) and R ($1\bar{1}02$) planes in parallel (black curve) and perpendicular (red curve) polarizations, b) Corresponding Fourier Transforms (Δk = 4-9.5 Å^{-1}) uncorrected for phase shift.

The size of MoS_2 slabs can be potentially determined based on the coordination number of Mo second neighbors [45,51]. In fact, a coordination number of 1-2 as found above for model catalysts should correspond to a slab size of about 1-2 nm following the model of Shido and Prins [51]. This size is clearly underestimated with respect to TEM analysis (Fig. 8) and this discrepancy has been largely debated in the literature and explained by several effects including a high degree of disorder and/or existence of TEM-invisible small MoS_2 particles [45,51].

The EXAFS signal was very weakly affected by changing the polarization for the A ($11\bar{2}0$), M ($10\bar{1}0$) and R ($1\bar{1}02$) planes as already observed for the XANES region, meaning that MoS_2 slabs are not specifically oriented on these surfaces. Conversely, a more noticeable polarization effect is observed for the C (0001) plane in line with XANES results. The FT (Figure 10) shows that the intensity of the second shell (Mo neighbors) is higher for the

parallel polarization. Quantitative fitting yields a coordination number of 1.8 Mo in parallel polarization and 0.8 Mo in perpendicular polarization.

This difference can be explained by a preferential orientation of MoS_2 slabs parallel to the surface. One hypothesis could involve a basal bonding of MoS_2 slabs on the support (Scheme 2). In this case, Mo-Mo bonds are parallel to the electric field vector in parallel polarization leading to an enhancement of the Mo-Mo contribution. In perpendicular polarization, Mo-Mo linkages are perpendicular to the electric field vector which explains a decrease of the Mo-Mo contribution. However, if all MoS_2 slabs were basal bonded, the Mo-Mo contribution should completely vanish in perpendicular polarization. Since the second Mo shell is present for both polarizations, it is more likely that only part of MoS_2 slabs are basal bonded while another part is randomly oriented. It can be inferred that basal bonded slabs are the largest ones while the smallest ones are randomly oriented. Another alternative hypothesis would involve a tilted geometry for 100% of MoS_2 slabs with respect to the surface. However, this hypothesis appears much less plausible since AFM (Figure 6) showed a rather heterogeneous distribution of MoS_2 on the surface which is not in agreement with a unique orientation of MoS_2 clusters.

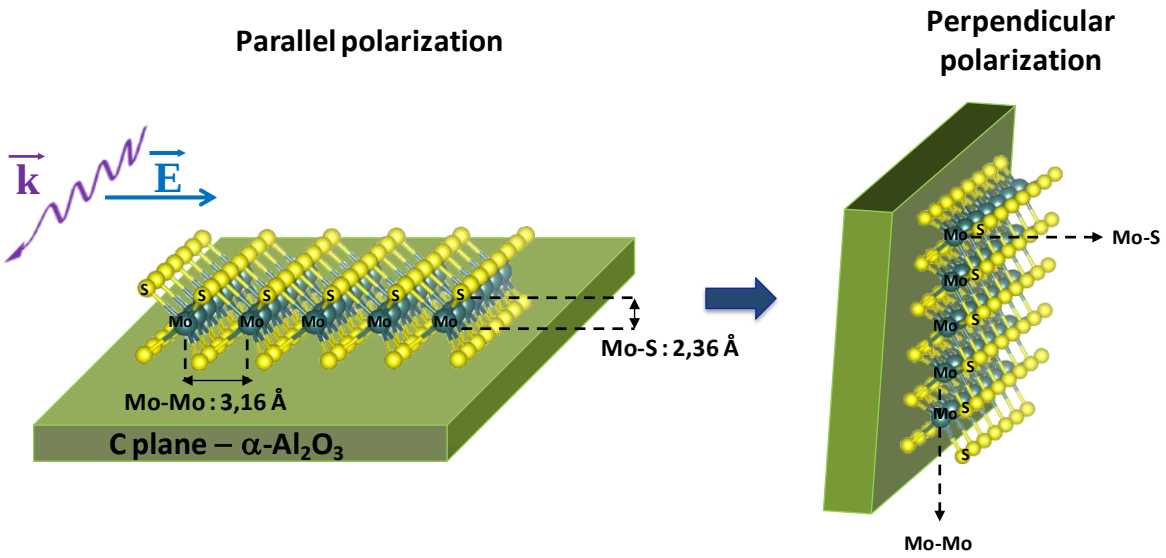

Scheme 2: Basal orientation of MoS_2 slabs on the C (0001) plane of α-Al_2O_3 and change of polarization with respect to the synchrotron beam: parallel on the left and perpendicular on the right. $\vec{k}$ is the wave vector and $\vec{E}$ is the electric field vector.

It has been established in the preceeding sections that metal-support interactions are weak on the C (0001) plane. In fact, this conclusion is in full agreement with the basal bonding

discussed above since it has been shown by DFT calculations that the absence of specific interactions between the active phase and the support will favor a basal orientation of MoS_2 [52,53].

Sulfide model catalysts have also been analyzed by HR HAADF-STEM in order to confirm the orientation of MoS_2 slabs determined by GI-EXAFS. In fact, with STEM in the HAADF detection mode, intensity is proportional to the squared atomic number (Z^2) of the observed atoms [54,55], making feasible the detection of MoS_2 slabs oriented perpendicular to the incident electron beam and thus parallel to the surface and possibly the determination of the associated 2D morphology [56–59]. The analysis was also performed on samples sulfided at 300 °C to compare HAADF-STEM images to GI-EXAFS results.

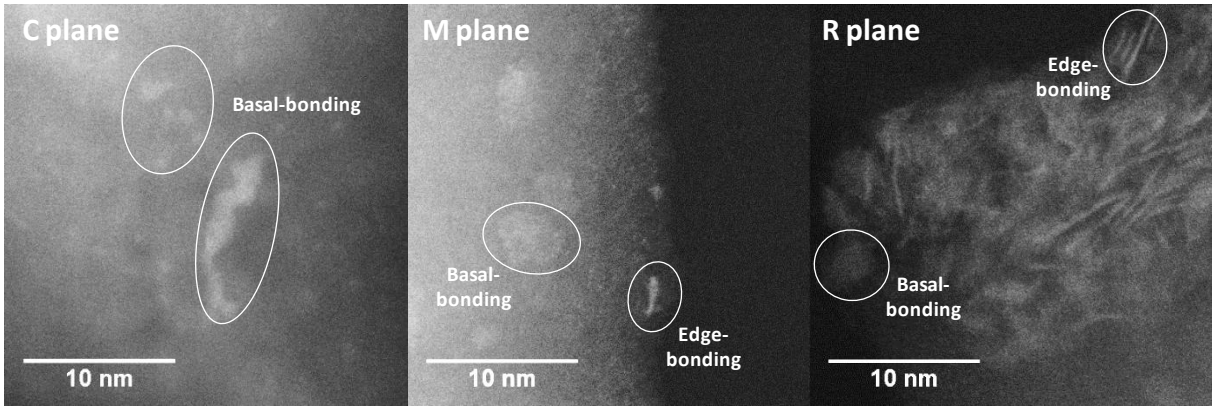

Figure 11: Typical HR HAADF-STEM images of sulfided model Mo/α-Al_2O_3 catalysts (Mo surface loading is 3.5 at.nm^{-2}) supported on the C (0001), M ($10\bar{1}0$) and R ($1\bar{1}02$) orientations of α-Al_2O_3. Samples were prepared by Mo impregnation, calcination at 450°C for 2h and sulfidation at 300°C under H_2S/H_2.

On the C (0001) plane, a preferential basal orientation of MoS_2 slabs was observed (Figure 11) in full agreement with XAS results. The average slab size is also larger (with a distribution in the 2-6 nm range) with respect to the other orientations as shown previously by TEM (Figure 8). On the M ($10\bar{1}0$) plane, STEM images show a random orientation with a similar ratio of edge and basal bonded MoS_2 slabs (Figure 11) wich confirms the absence of polarization effect in XAS. One-layer thick MoS_2 slabs are predominant on this surface as reported by TEM. Finally, on the R ($1\bar{1}02$) surface, STEM results are less straightforward than with TEM and AFM. One-layer thick MoS_2 slabs are observed which are mostly basal bonded with a size distribution in the range of 1-4 nm in good agreement with TEM analysis.

However, there is also another group of edge-bonded MoS_2 clusters with a higher stacking degree (up to 6) and larger average size around 8 nm suggesting that this sample is probably more heterogeneous than the one observed with conventional TEM.

Nevertheless, HAADF-STEM observations are qualitatively in line with GI-EXAFS and confirm the support effect on the orientation of the active phase: predominant basal orientation on the C (0001) plane and random (basal and edge bonding) on the M ($10\bar{1}0$) and R ($1\bar{1}02$) planes.

5. Influence of synthesis route: equilibrium adsorption vs impregnation

The results reported in the present contribution are related to model catalysts prepared by a simple *impregnation* of Mo in order to mimic the classical incipient wetness impregnation used for industrial catalysts. These results, especially sulfidation degree, can be compared to our previous study on the same type of model systems but prepared by *equilibrium adsorption* (selective adorption) [11]. The latter technique is more selective since only specifically adsorbed species remain on the surface thanks to a washing step which removes weakly bound Mo species.

This comparison will be focused on the A ($11\bar{2}0$) and R ($1\bar{1}02$) orientations since i) the C (0001) plane is not adsorbing Mo through equilibrium adsorption [11] and ii) the A ($11\bar{2}0$) and M ($10\bar{1}0$) planes show a similar behavior due to the same type of surface hydroxyls [8]. The Mo loading investigated is different for the two surfaces considered since the nature and number of each surface adsorption sites are different and hence, the maximum Mo surface density that can be reached by equilibrium adsorption is also different (i.e about 3.5 at.nm^{-2} for the A ($11\bar{2}0$) plane and 1.0 at.nm^{-2} for the R ($1\bar{1}02$) plane).

Figure 12 compares the sulfidation degree for both orientations and for both deposition methods. On both planes, the sulfidation degree is always lower for equilibrium adsorption for all sulfidation temperatures: about 10 to 20 % lower for the A ($11\bar{2}0$) plane and 20 to 30 % for the R ($1\bar{1}02$) plane. These differences are the highest for the surface showing the strongest metal-support interactions.

These differences may be explained by a more homogeneous spreading of polyoxo Mo species on the surface through equilibrium adsorption due to the deposition procedure: large

volume of solution, long equilibration time (5 h). Moreover, the washing step removes non-chemically adsorbed Mo species that would be easier to sulfide. Hence, all other things being equal, equilibrium adsorption will lead to more evenly spread molybdates in stronger interaction with the surface, probably via Al-O-Mo chemical bonds and consequently to a lower sulfidation degree as compared to impregnation.

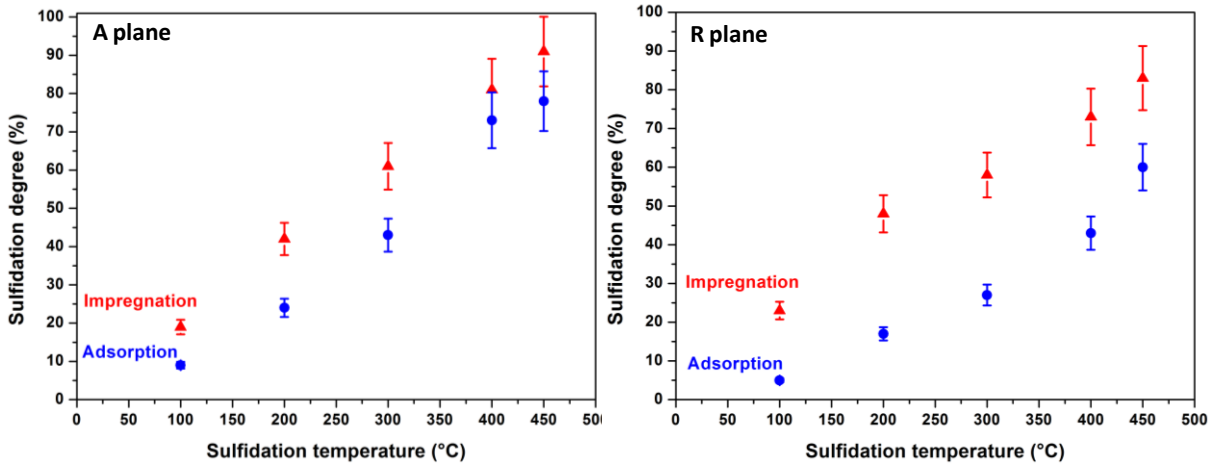

Figure 12: Comparison of sulfidation degree as a function of sulfidation temperature for model Mo/α-Al_2O_3 catalysts prepared by impregnation (red triangles) and by equilibrium adsorption (blue circles) on the A $(11\bar{2}0)$ plane (Mo loading of 3.5 at.nm^{-2}) and on the R $(1\bar{1}02)$ plane (Mo loading of 1.0 at.nm^{-2}).

6. From model systems to industrial catalysts

We have shown previously [8,11] that the different α-Al_2O_3 orientations investigated in the present work can be taken as reasonable models for the various surfaces exhibited by γ-Al_2O_3, the conventional support for HDS catalysis. Detailed analysis of the surface hydroxyl groups exposed by the α and γ-Al_2O_3 polymorphs has enabled the following analogies: [8,11] the predominant (110) γ-Al_2O_3 surface can be (at least partially) modeled by the R $(1\bar{1}02)$ plane (both expose Al_{4c}-μ_1-OH surface sites); the (100) γ-Al_2O_3 surface can be modeled by the A $(11\bar{2}0)$ and M $(10\bar{1}0)$ orientations (both expose Al_{6c}-μ_1-OH and Al_{6c}-μ_3-OH surface sites) and finally the speciation of surface OH on the (111) γ-Al_2O_3 surface (singly, doubly and triply coordinated surface OH) is a combination of that on the A $(11\bar{2}0)$, C (0001) and M $(10\bar{1}0)$ surfaces. The proposed surface relationship between α and γ–Al_2O_3 orientations is represented schematically in Scheme 3. Following this approach, the results reported in the present work allow us to propose a comprehensive picture of the Mo speciation at the oxide

and sulfide states on the various α orientations and to extend these results to γ–Al_2O_3 (Scheme 3).

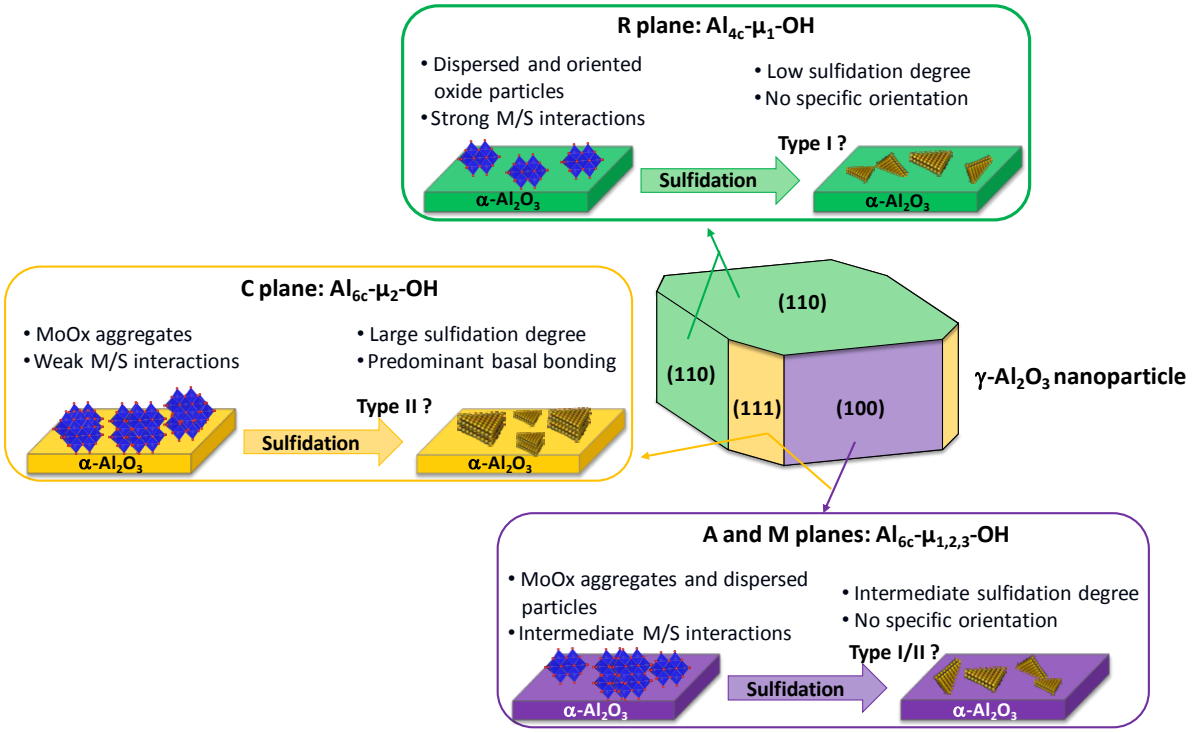

Scheme 3: Surface-dependent speciation of Mo species (at the oxide and sulfide state) on α-Al_2O_3 surfaces based on the results described in this work and proposed relationship with γ-Al_2O_3 by taking into account the speciation of surface OH[14] and the morphology of γ-Al_2O_3 particles as shown in Digne et *al.*[60] M/S stands for Metal/Support.

Weak metal-support interactions are assumed on the C (0001) plane leading to the formation of Mo oxide aggregates after calcination that will be easily sulfided and will eventually form large and stacked MoS_2 slabs predominantly basal bonded as shown by GI-EXAFS and HAADF-STEM. These results are in full agreement with the proposal of Sakashita [10] based on results obtained on thin (111) γ-Al_2O_3 films implying the formation of stacked MoS_2 slabs basal bonded to the support. Using the concept of type I/type II active phase [61,62], MoS_2 slabs could be associated to type II on the C (0001) plane, i.e. weaker metal-support interactions and higher activity than type I. However, this analogy has to be restrained since i) type II structures do not necessarily involve multi-stacked slabs [61,62] and ii) the size of the slabs are another key parameter since large particles (as on the C (0001) plane) will have a reduced number of edge sites leading to lower catalytic activity.

On A (11$\bar{2}$0) and M (10$\bar{1}$0) planes, stronger metal-support interactions are postulated leading to shorter and less stacked MoS_2 slabs and to lower sulfidation degree with respect to the C (0001) facet. As a consequence the nature of the active phase is different on the A (11$\bar{2}$0)/M (10$\bar{1}$0) planes and on the C (0001) plane. Hence, this dissimilarity is in disagreement with our previous assumption [11] that the sulfide phase was of type II on A (11$\bar{2}$0)/M (10$\bar{1}$0)planes and therefore on the (100) plane of γ-Al_2O_3. The situation is probably more complex with an intermediate case between type I and type II structures. Furthermore, it has to be noted that our results are at variance with the work of Sakashita [10] who suggested a perpendicular orientation of MoS_2 slabs on the (100) γ-Al_2O_3 surface while our GI-EXAFS and HAADF-STEM results reveal a random orientation of MoS_2 slabs (i.e basal and edge bonding).

Finally, the strongest metal/support interactions are observed on the R (1$\bar{1}$02) plane with a homogeneous dispersion (AFM) and specific orientation (GI-EXAFS) of Mo oxide nanoparticles. Conversely, no specific orientation of MoS_2 slabs has been found from GI-EXAFS analysis suggesting that restructuring of the supported Mo phase occurs during sulfidation. Low sulfidation degree along with small and weakly stacked MoS_2 slabs could be associated to type I structures on this surface and the associated (110) γ-Al_2O_3 surface.

Conclusions

A model approach has been followed in order to gain a molecular-scale insight into the Mo speciation at the oxide and sulfide states in alumina-supported hydrotreating catalysts. Several α-Al_2O_3 surfaces with different orientations (A (11$\bar{2}$0), C (0001), M (10$\bar{1}$0) and R (1$\bar{1}$02)) were used as surrogates for γ-Al_2O_3. The surface relationship between α and γ-Al_2O_3 polymorphs is summarized in Scheme 3.

Mo deposition was performed by impregnation to mimic industrial catalyst synthesis procedure and to get a proper control of the molybdenum surface density which facilitates comparison between model surfaces.

AFM characterization of the calcined catalysts reveals different dispersions for Mo oxide nanoparticles which can be related to the strength of metal-support interactions. Three differents behaviors have been documented: i) weak metal-support interactions on the C (0001) plane, ii) intermediate on A (11$\bar{2}$0) and M (10$\bar{1}$0) planes and iii) strong on the

R ($1\bar{1}02$) plane that can be related to speciation of surface hydroxyls. A specific orientation of Mo oxide species has also been pointed out by GI-XAS spectroscopy on the R ($1\bar{1}02$) plane revealing a structuring effect of the facet in agreement with the high strength of metal-support interactions.

The Mo sulfidation capacity on each model surface is a direct consequence of the previous findings. A maximum sulfidation degree (90 %) at low temperature (300°C) was observed for the C (0001) plane with a larger MoS_2 slab size and stacking as compared to A ($11\bar{2}0$), M ($10\bar{1}0$) and R ($1\bar{1}02$) facets. A predominant basal orientation of MoS_2 slabs on the C (0001) plane was also pointed out by GI-EXAFS in agreement with the absence of specific metal-support interactions while a random orientation was observed for the other surfaces. A ($11\bar{2}0$), and M ($10\bar{1}0$) surfaces present an intermediate sulfidation degree while the R ($1\bar{1}02$) plane shows the weakest sulfidation degree and MoS_2 slab size.

Comparison among preparation routes (i.e equilibrium adsorption vs. impregnation) indicates that equilibrium adsorption leads to the weakest sulfidation degree which can be explained by Mo species in stronger interaction with the surface due to a more efficient spreading during deposition.

Extension of these results to γ alumina suggests a surface-dependent Mo sulfidation and orientation on industrial hydrotreating catalysts. They confirm that the precise control of the alumina morphology might lead to more active catalyst.

Supporting Information

Supplementary data associated with this article can be found: quantitative EXAFS analysis of sulfided model Mo/α-Al_2O_3 catalysts.

Acknowledgements

We gratefully acknowledge C. Méthivier and C. Calers for assistance in XPS analysis and S. Casale for TEM experiments. GI-XAS Experiments were performed on the Samba beamline at SOLEIL Synchrotron (France) under proposal number 20131167. We are grateful to the SAMBA beamline staff for valuable help. We express gratitude to O. Ersen for his

contribution to HAADF-STEM analyses at the Université de Strasbourg (IPCMS-UMR 7504 CNRS).

References

[1] H. Toulhoat, P. Raybaud, Catalysis by transition metal sulphides from molecular theory to industrial application, Technip, Paris, France, (2013).

[2] C. Song, An overview of new approaches to deep desulfurization for ultra-clean gasoline, diesel fuel and jet fuel., Catal. Today. 86 (2003) 211–263.

[3] E. Furimsky, Hydroprocessing challenges in biofuels production., Catal. Today. 217 (2013) 13–56.

[4] R. Prins, in Handbook of Heterogeneous Catalysis, G. Ertl, H. Knözinger, F. Schüth (Eds.), Wiley-VCH Verlag, Weinheim, (1997), vol 4.

[5] H. Topsøe, B.S. Clausen, F. Massoth, in Hydrotreating Catalysis Science and Technology, J.R. Anderson, M. Boudart (Eds.), Springer Berlin Heidelberg (1996), vol 11.

[6] H. Topsøe, B.S. Clausen, R. Candia, C. Wivel, S. Mørup, In situ Mössbauer emission spectroscopy studies of unsupported and supported sulfided cobalt-molybdenum hydrodesulfurization catalysts: evidence for and nature of a cobalt-molybdenum-sulfur phase., J. Catal. 68 (1981) 433–452.

[7] D. Laurenti, B. Phung-Ngoc, C. Roukoss, E. Devers, K. Marchand, L. Massin, L. Lemaitre, C. Legens, A.-A. Quoineaud, M. Vrinat, Intrinsic potential of alumina-supported CoMo catalysts in HDS: Comparison between γ_c, γ_T, and δ-alumina., J. Catal. 297 (2013) 165–175.

[8] C. Bara, E. Devers, M. Digne, A.-F. Lamic-Humblot, G. Pirngruber, X. Carrier, A review of surface science approaches for the preparation of alumina-supported hydrotreating catalysts., ChemCatChem. 7 (2015) 3422-3440.

[9] Y. Sakashita, T. Yoneda, Orientation of MoS_2 clusters supported on two kinds of γ-Al_2O_3 single crystal surfaces with different indices., J. Catal. 185 (1999) 487–495.

[10] Y. Sakashita, Effects of surface orientation and crystallinity of alumina supports on the microstructures of molybdenum oxides and sulfides., Surf. Sci. 489 (2001) 45–58.

[11] C. Bara, L. Plais, K. Larmier, E. Devers, M. Digne, A.-F. Lamic-Humblot, G.D. Pirngruber, X. Carrier, Aqueous-phase preparation of model HDS catalysts on planar alumina substrates: support effect on Mo adsorption and sulfidation., J. Am. Chem. Soc. 137 (2015) 15915–15928.

[12] A.D. Gandubert, C. Legens, D. Guillaume, E. Payen, X-ray photoelectron spectroscopy surface quantification of sulfided CoMoP catalysts. Relation between activity and promoted sites. Part II: Influence of the sulfidation temperature., Surf. Interface Anal. 38 (2006) 206–209.

[13] C.A. Schneider, W.S. Rasband, K.W. Eliceiri, NIH image to imageJ: 25 years of image analysis., Nat. Methods 9 (2012), 671-675.

[14] J. Adamcik, A. Berquand, R. Mezzenga, Single-step direct measurement of amyloid fibrils stiffness by peak force quantitative nanomechanical atomic force microscopy., Appl. Phys. Lett. 98 (2011) 193701/1-193701/3.

[15] F. Baudelet, R. Belkhou, V. Briois, A. Coati, P. Dumas, V. Etgens, A.M. Flank, P. Fontaine, Y. Garreau, I. Quinkal, F. Rochet, P. Roy, M. Sauvage, F. Sirotti, A. Somogyi, D. Thiaudère, SOLEIL, un nouvel outil puissant pour les sciences des matériaux, Oil Gas Sci. Technol. - Rev IFP. 60 (2005) 849–874.

[16] B. Ravel, M. Newville, ATHENA, ARTEMIS, HEPHAESTUS: data analysis for x-ray absorption spectroscopy using IFEFFIT., J. Synch. Rad. 12 (2005) 537–541.

[17] M. Shirai, Y. Iwasawa, in X-ray absorption fine stucture for catalysts and surfaces, Y. Iwasawa, (Ed), World Scientific, Singapore, 1996, p.332.

[18] L. Wiehl, J. Oster, M. Huth, High-resolution transmission electron microscopic investigations of molybdenum thin films on faceted α-Al_2O_3., J. Appl. Crystallogr. 38 (2005) 260–265.

[19] J.R. Heffelfinger, C.B. Carter, Mechanisms of surface faceting and coarsening., Surf. Sci. 389 (1997) 188–200.

[20] S. Curiotto, D. Chatain, Surface morphology and composition of c-, a- and m-sapphire surfaces in O_2 and H_2 environments., Surf. Sci. 603 (2009) 2688–2697.

[21] S.C. Parker, C.T. Campbell, Kinetic model for sintering of supported metal particles with improved size-dependent energetics and applications to Au on TiO_2(110)., Phys. Rev. B Condens. Matter Mater. Phys. 75 (2007) 035430/1-035430/15.

[22] C.T. Campbell, J.C. Sharp, Y.X. Yao, E.M. Karp, T.L. Silbaugh, Insights into catalysis by gold nanoparticles and their support effects through surface science studies of model catalysts., Faraday Discuss. 152 (2011) 227–239.

[23] C.H. Bartholomew, in Studies in Surface Science and Catalysis, C.H. Bartholomew and G.A. Fuentes (Eds.), Elsevier, (1997) pp. 585–592.

[24] C.T. Campbell, The Energetics of Supported Metal Nanoparticles: Relationships to Sintering Rates and Catalytic Activity., Acc. Chem. Res. 46 (2013) 1712–1719.

[25] A. Tougerti, E. Berrier, A.-S. Mamede, C. La Fontaine, V. Briois, Y. Joly, E. Payen, J.-F. Paul, S. Cristol, Synergy between XANES Spectroscopy and DFT to Elucidate the Amorphous Structure of Heterogeneous Catalysts: TiO_2 -Supported Molybdenum Oxide Catalysts., Angew. Chem. Int. Ed. 52 (2013) 6440–6444.

[26] M. de Boer, A.J. van Dillen, D.C. Koningsberger, J.W. Geus, M.A. Vuurman, I.E. Wachs, Remarkable spreading behavior of molybdena on silica catalysts: an in situ EXAFS-Raman study., Catal. Lett. 11 (1991) 227–239.

[27] A. Tougerti, I. Llorens, F. D'Acapito, E. Fonda, J.-L. Hazemann, Y. Joly, D. Thiaudière, M. Che, X. Carrier, Surface Science Approach to the Solid-Liquid Interface: Surface-Dependent Precipitation of $Ni(OH)_2$ on α-Al_2O_3 Surfaces., Angew. Chem. Int. Ed. 51 (2012) 7697–7701.

[28] M. Shirai, Polarized Total-Reflection Fluorescence EXAFS Study of Anisotropic Structure Analysis for Co Oxides on α-Al_2O_3 (0001) as Model Surfaces for Active Oxidation Catalysts., J. Catal. 145 (1994) 159–165.

[29] W.-J. Chun, K. Asakura, Y. Iwasawa, Polarization-dependent total-reflection fluorescence XAFS study of Mo oxides on a rutile TiO_2(110) single crystal surface., J. Phys. Chem. B. 102 (1998) 9006–9014.

[30] H.T. Evans, B.M. Gatehouse, P. Leverett, Crystal structure of the heptamolybdate(VI) (paramolybdate) ion, $[Mo_7O_{24}]^{6-}$ in the ammonium and potassium tetrahydrate salts., J. Chem. Soc. Dalton Trans. (1975) 505-514.

[31] X. Carrier, E. Marceau, M. Che, Physical techniques and catalyst preparation: Determining the interactions of transition-metal complexes with oxide surfaces., Pure Appl. Chem. 78 (2006) 1039–1055.

[32] D.C. Koningsberger, R. Prins, eds., X-ray absorption: principles, applications, techniques of EXAFS, SEXAFS, and XANES., Wiley, New York, 1988.

[33] B.S. Clausen, B. Lengeler, H. Topsøe, X-ray absorption spectroscopy studies of calcined Mo/Al_2O_3 and $CoMo/Al_2O_3$ hydrodesulfurization catalysts., Polyhedron. 5 (1986) 199–202.

[34] R.G. Leliveld, A.J. van Dillen, J.W. Geus, D.C. Koningsberger, A Mo–K Edge XAFS Study of the Metal Sulfide-Support Interaction in (Co) Mo Supported Alumina and Titania Catalysts., J. Catal. 165 (1997) 184–196.

[35] C. Geantet, E. Payen, in Catalysis by transition metal sulphides from molecular theory to industrial application., Raybaud, H. Toulhoat (Eds.), Technip, (2013) pp. 274–300.

[36] J.C. Muijsers, T. Weber, R.M. van Hardeveld, H.W. Zandbergen, J.W. Niemantsverdriet, Sulfidation study of molybdenum oxide using $MoO_3/SiO_2/Si$(100) model catalysts and Mo_3^{IV}-sulfur cluster compounds., J. Catal. 157 (1995) 698–705.

[37] T. Weber, J.C. Muijsers, J. van Wolput, C.P.J. Verhagen, J.W. Niemantsverdriet, Basic reaction steps in the sulfidation of crystalline MoO_3 to MoS_2, as studied by X-ray photoelectron and infrared emission spectroscopy., J. Phys. Chem. 100 (1996) 14144–14150.

[38] A.D. Gandubert, C. Legens, D. Guillaume, S. Rebours, E. Payen, X-ray Photoelectron Spectroscopy Surface Quantification of Sulfided CoMoP Catalysts – Relation Between Activity and Promoted Sites – Part I: Influence of the Co/Mo Ratio., Oil Gas Sci. Technol. - Rev. IFP. 62 (2007) 79–89.

[39] A.D. Gandubert, E. Krebs, C. Legens, D. Costa, D. Guillaume, P. Raybaud, Optimal promoter edge decoration of CoMoS catalysts: A combined theoretical and experimental study., Catal. Today. 130 (2008) 149–159.

[40] L.P. Hansen, E. Johnson, M. Brorson, S. Helveg, Growth Mechanism for Single- and Multi-Layer MoS_2 Nanocrystals., J. Phys. Chem. C. 118 (2014) 22768–22773.

[41] F. Cesano, S. Bertarione, A. Piovano, G. Agostini, M.M. Rahman, E. Groppo, F. Bonino, D. Scarano, C. Lamberti, S. Bordiga, L. Montanari, L. Bonoldi, R. Millini, A. Zecchina, Model oxide supported MoS_2 HDS catalysts: structure and surface properties., Catal. Sci. Technol. 1 (2011) 123-136.

[42] M. Boudart, R.A. Dalla Betta, K. Foger, D.G. Loffler, M.G. Samant, Study by synchrotron radiation of the structure of a working catalyst at high temperatures and pressures., Science 228 (1985) 717–719.

[43] B.S. Clausen, H. Topsøe, R. Candia, J. Villadsen, B. Lengeler, J. Als-Nielsen, F. Christensen, Extended x-ray absorption fine structure study of the cobalt-molybdenum hydrodesulfurization catalysts., J. Phys. Chem. 85 (1981) 3868–3872.

[44] R.G. Leliveld, A.J. van Dillen, J.W. Geus, D.C. Koningsberger, The sulfidation of γ-alumina and titania supported (cobalt)molybdenum oxide catalysts monitored by EXAFS., J. Catal. 171 (1997) 115–129.

[45] C. Calais, N. Matsubayashi, C. Geantet, Y. Yoshimura, H. Shimada, A. Nishijima, M. Lacroix, M. Breysse, Crystallite size determination of highly dispersed unsupported MoS_2 catalysts., J. Catal. 174 (1998) 130–141.

[46] H. Shimada, N. Matsubayashi, T. Sato, Y. Yoshimura, M. Imamura, T. Kameoka, A. Nishijima, EXAFS study on the dispersion of molybdenum sulfide catalysts on γ-alumina., Catal. Lett. 20 (1993) 81–86.

[47] G.U. Kulkarni, C.N.R. Rao, EXAFS study of the molybdenum/titania hydrodesulfurization catalysis., Catal. Lett. 11 (1991) 63–70.

[48] Y. Yoshimura, N. Matsubayashi, T. Sato, H. Shimada, A. Nishijima, Molybdate catalysts prepared by a novel impregnation method: effect of citric acid has a ligand on the catalytic activities., Appl. Catal. Gen. 79 (1991) 145–159.

[49] N. Matsubayashi, H. Shimada, T. Sato, Y. Yoshimura, M. Imamura, A. Nishijima, Structural change of supported Ni-Mo sulfide catalysts during the hydrogenation of coal-derived liquids., Fuel Process. Technol. 41 (1995) 261–271.

[50] Y. Yokoyama, N. Ishikawa, K. Nakanishi, K. Satoh, A. Nishijima, H. Shimada, N. Matsubayashi, M. Nomura, Deactivation of Co-Mo/Al_2O_3 hydrodesulfurization catalysts during a one-year commercial run., Catal. Today. 29 (1996) 261–266.

[51] T. Shido, R. Prins, Why EXAFS underestimated the size of small supported MoS_2 particles., J. Phys. Chem. B. 102 (1998) 8426–8435.

[52] D. Costa, C. Arrouvel, M. Breysse, H. Toulhoat, P. Raybaud, Edge wetting effects of γ-Al_2O_3 and anatase-TiO_2 supports by MoS_2 and CoMoS active phases: A DFT study., J. Catal. 246 (2007) 325–343.

[53] C. Arrouvel, M. Breysse, H. Toulhoat, P. Raybaud, A density functional theory comparison of anatase (TiO_2)- and γ-Al_2O_3-supported MoS_2 catalysts., J. Catal. 232 (2005) 161–178.

[54] D.E. Jesson, S.J. Pennycook, Incoherent imaging of crystals using thermally scattered electrons., Proc. Math. Phys. Sci. 449 (1995) 273–293.

[55] P.D. Nellist, S.J. Pennycook, Direct Imaging of the Atomic Configuration of Ultradispersed Catalysts., Science. 274 (1996) 413–415.

[56] A. Carlsson, M. Brorson, H. Topsøe, Supported metal sulphide nanoclusters studied by HAADF-STEM, J. Microsc. 223 (2006) 179–181.

[57] T. Alphazan, A. Bonduelle-Skrzypczak, C. Legens, A.-S. Gay, Z. Boudene, M. Girleanu, O. Ersen, C. Copéret, P. Raybaud, Highly Active Nonpromoted Hydrotreating Catalysts through the Controlled Growth of a Supported Hexagonal WS_2 Phase., ACS Catal. 4 (2014) 4320–4331.

[58] M. Girleanu, T. Alphazan, Z. Boudene, A. Bonduelle-Skrzypczak, C. Legens, A.-S. Gay, C. Coperet, O. Ersen, P. Raybaud, Magnifying the Morphology Change Induced by a

Nickel Promoter in Tungsten(IV) Sulfide Industrial Hydrocracking Catalyst: A HAADF-STEM and DFT Study., ChemCatChem. 6 (2014) 1594–1598.

[59] B. Baubet, M. Girleanu, A.-S. Gay, A.-L. Taleb, M. Moreaud, F. Wahl, V. Delattre, E. Devers, A. Hugon, O. Ersen, P. Afanasiev, P. Raybaud, Quantitative Two-Dimensional (2D) Morphology-Selectivity Relationship of CoMoS Nanolayers: A Combined High-Resolution High-Angle Annular Dark Field Scanning Transmission Electron Microscopy (HR HAADF-STEM) and Density Functional Theory (DFT) Study., ACS Catal. 6 (2016) 1081–1092.

[60] M. Digne, P. Sautet, P. Raybaud, P. Euzen, H. Toulhoat, Use of DFT to achieve a rational understanding of acid-basic properties of γ-alumina surfaces, J. Catal. 226 (2004) 54–68.

[61] R. Candia, O. Soerensen, J. Villadsen, N.Y. Topsøe, B.S. Clausen, H. Topsøe, Effect of sulfiding temperature on activity and structure of cobalt-molybdenum/γ-alumina catalysts. II., Bull. Soc. Chim. Belg. 93 (1984) 763–773.

[62] B. Hinnemann, J.K. Nørskov, H. Topsøe, A density functional study of the chemical differences between Type I and Type II MoS_2-based structures in hydrotreating catalysts., J. Phys. Chem. B. 109 (2005) 2245–2253.